Non-radiative energy transfer and selective charge transfer in a WS2/(PEA)2PbI4 heterostructure

Karpińska, M.; Liang, M.; Kempt, R.; Finzel, K.; Kamminga, M.; Zhang, N.; Knodlseder, C.; Maude, D. K.; Baranowski, M.; Łopotowski, Ł.; Ye, J.; Kuc, A. B.; Plochocka, P.;

Originally published:

July 2021

ACS Applied Materials and Interfaces 13(2021)28, 33677-33684

DOI: https://doi.org/10.1021/acsami.1c08377

Non-radiative energy transfer and selective charge transfer in a $WS_2/(PEA)_2PbI_4$ heterostructure

Miriam Karpińska,[†,‡] Minpeng Liang,[¶] Roman Kempt,[§] Kati Finzel,[§] Machteld Kamminga,[¶] Nan Zhang,[†] Catherine Knodlseder,[†] Duncan K. Maude,[†] Michał Baranowski,[‖] Łukasz Kłopotowski,[‡] Jianting Ye,[¶] Agnieszka Kuc,[*,⊥] and Paulina Plochocka[*,†,‖]

†*Laboratoire National des Champs Magnétiques Intenses, UPR 3228, CNRS-UGA-UPS-INSA, Grenoble and Toulouse, France*
‡*Institute of Physics, Polish Academy of Sciences, 02-668 Warsaw, Poland*
¶*Zernike Institute for Advanced Materials, University of Groningen, Nijenborgh 4, 9747 AG Groningen, The Netherlands*
§*Technische Universität Dresden, Bergstr. 66c, 01062 Dresden, Germany*
‖*Department of Experimental Physics, Faculty of Fundamental Problems of Technology, Wroclaw University of Science and Technology, Wroclaw, Poland*
⊥*Helmholtz-Zentrum Dresden-Rossendorf, Bautzner Landstrasse 400, 01328 Dresden, Germany*

E-mail: a.kuc@hzdr.de; paulina.plochocka@lncmi.cnrs.fr

Abstract

van der Waals heterostructures are currently the focus of intense investigation, this is essentially due to the unprecedented flexibility offered by the total relaxation of lattice matching requirements, and their new and exotic properties compared to the individual layers. Here, we investigate the hybrid transition metal dichalcogenide/2D perovskite heterostructure $WS_2/(PEA)_2PbI_4$. We present the first DFT calculations of a heterostructure ensemble, which reveal a novel band alignment, where direct electron transfer is blocked by the organic spacer of the 2D perovskite. In contrast, the valence band forms a cascade from WS_2 through the PEA to the PbI_4 layer allowing hole transfer. These predictions are supported by optical spectroscopy studies, which provide compelling evidence for both charge transfer, and non-radiative transfer of the excitation (energy transfer) between the layers. Our results show that TMD/2D perovskite heterostructures provide a flexible and convenient way to engineer the band alignment.

Introduction

Two dimensional (2D) layered materials have been in the scientific spotlight for more than a decade.[1,2] The seminal work of Geim and Novosolov on graphene,[3,4] was followed by the rediscovery of transition metal dichalcogenides (TMDs),[5,6] the recent explosion of the field of 2D perovskites,[7,8] and other emerging layered materials.[9,10] While initially the investigations of electronic properties were limited to monolayers within a particular group of materials, recently, the engineering of van der Waals stacks has attracted tremendous attention.[11–16] The inherently weak van der Waals interaction be-

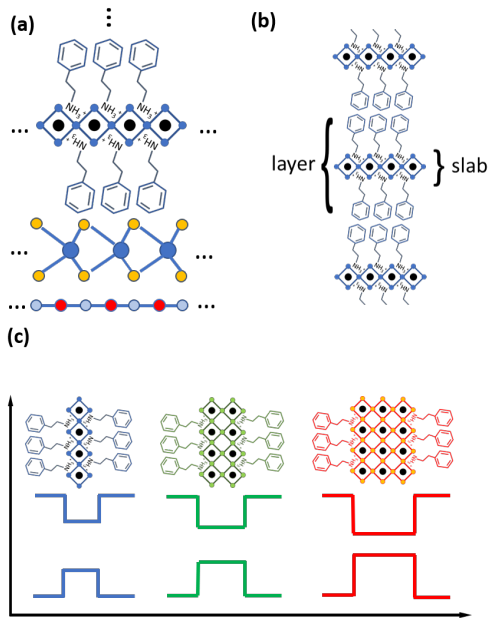

Figure 1: (a) Schematic of the investigated structure. On a h-BN layer, a monolayer of WS_2 is deposited, followed by a multilayer of $(PEA)_2PbI_4$ (PEPI) which is encapsulated by a top layer h-BN (not shown). (b) Schematic of the 2D perovskite structure with a single slab of inorganic octahedral units PbI_6 separated by organic spacers. (c) Schematic of the type-I band alignment of the perovskite with different thickens of the inorganic layers.

tween the 2D crystals facilitates the stacking of a variety of different layers into hetero- or homostructures[17,18] with new functional properties. The encapsulation of TMDs with h-BN results in superior electrical and optical quality. Stacking two different TMDs leads to a plethora of new properties, including long lived inter-layer excitons[19–21] which can be controlled by an electric or magnetic field,[22–24] and the formation of a moiré pattern[25,26] which can lead to exotic crystal phases.[12,27,28]

These functional properties strongly depend on the nature of the spatial excitation transfer between the layers, which can rely on charge transfer and/or energy transfer. For example, the type-II band alignment in TMD stacks[29] favours charge transfer, which leads to the formation of inter-layer excitons with new exotic properties.[12,25–27,30,31] On the other hand, stacks of 2D semiconductors, in principle, form an ideal platform to explore energy transfer (non-radiative transfer of the excitation). This is due to the large oscillator strength and ultimate proximity of the functional layers (in the range of single to few to dozen ofÅ), essential for nonradiative energy transfer of the Förster or Dexter type.[32–39] The energy transfer can be the dominant process if the direct inter-layer charge transfer is strongly suppressed. This can be achieved, for example, by separating TMD layers with an insulating sheet of h-BN.[39,40] The incorporation of different number of h-BN layers allows to control the mechanism of excitation transfer from a direct charge transfer to an energy transfer.[39–42]

Here, we propose a novel approach to control the excitation transfer process, using a hybrid heterostructure built from a TMD monolayer and a 2D perovskite $(PEA)_2PbI_4$ (PEPI),[7,8] which is presented schematically in Fig. 1(a). The 2D perovskite provides a charge blocking layer in the form of organic spacers. As we show here, such a stack can provide a rather unique band alignment, not achievable in TMD-based van der Waals heterostructures. Taking into account the plethora of available organic spacers that can be incorporated into the 2D perovskites,[7] this new approach to heterostructure design provides greater flexibility in the band alignment, together with the possibility to engineer the excitation transfer mechanism. The efficient energy transfer can be used to sensitize the photo-response of one layer (for example TMD) using the other layer (2D perovskite), without reduction of the overall photo-response yield characteristic for the inter-layer charge transfer and weak inter-layer emission.

Two-dimensional Ruddlesden-Popper type organic-inorganic perovskites consist of inorganic metal-halide octahedral slabs separated by large organic molecules (see Fig. 1(a)). They can be regarded as ideal quantum wells due to the lack of interface roughness and usually exhibit type-I band alignment (Fig. 1(c)), which prevents efficient charge transfer between the neighbouring slabs.[7,8,43,44] The thickness of the inorganic slab determines the optical band gap of such 2D perovskites, and can thus be used to sensitize TMDs monolayers to different photon energies. Interestingly, the character of the band gap does not depend on the slab thickness or the number of layers,[45,46] in contrast to the case of TMDs.[5] At the same time, 2D perovskites suffer from poor electrical properties (carrier mobility μ in the range of single

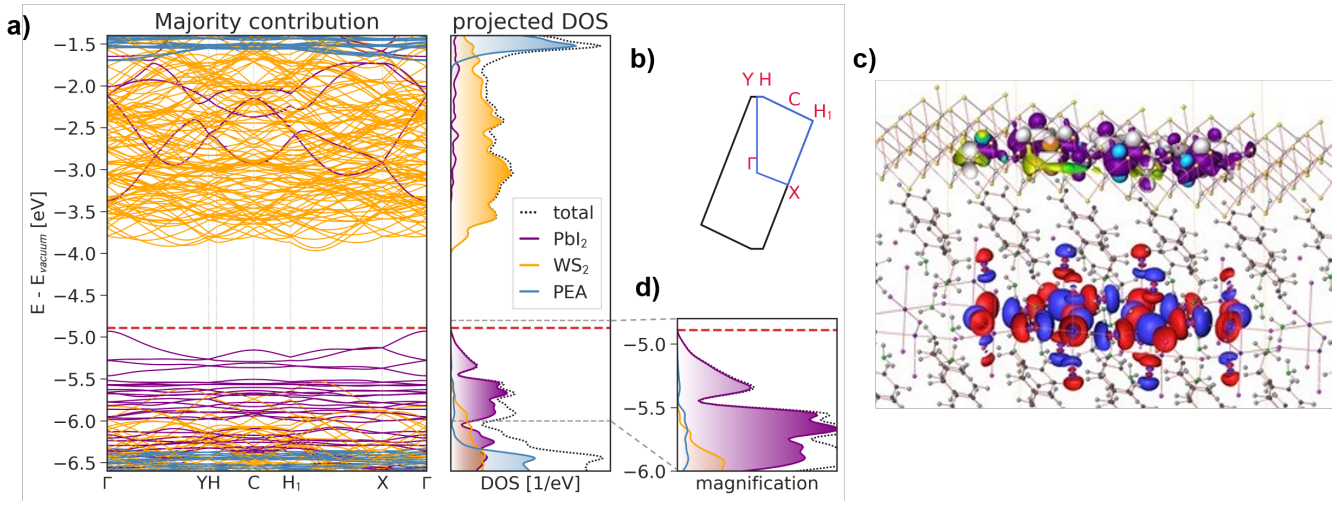

Figure 2: a) Mulliken-projected band structure of the WS_2/PEPI heterostructure showing the majority contributions of each layer and density of states projected to particular building blocks (WS_2, PEA, PbI_4). (b) The corresponding Brillouin zone and k-path of this low-symmetry model structure. Both band structure and density of states indicate type-II band alignment, which is also visible in the real-space representation of the highest-occupied and lowest-unoccupied crystal orbitals from the corresponding k-points in the band structure (c). The valence band maximum (VBM) is localized in the PbI_4 layer, while the conduction band minimum (CBM) is localized in the WS_2 layer. The orbitals are depicted using a 0.02 amplitude isosurface. For the real valued VBM at Γ, the negatives and positives are shown in blue and in red, respectively. In case of the complex valued CBM, the phase is indicated by the color map, ranging from -10^{-17} (violet) to 10^{-17} (white). (d) Magnification of the density of states close to the valance band to show the spurious contribution of organic ligand states.

$cm^2V^{-1}s^{-1}$) and TMDs are far better (2-3 order of magnitiud higher) in this respect.[47,48] Therefore, an appropriate utilization of charge or energy transfer can serve to suppress the drawbacks of individual layers, while enhancing their advantages, allowing for example, the creation of efficient photo-detectors.[49–52]

However, despite the potential advantages of TMDs/2D perovskite energy transfer heterostructures, very little is known about their properties, and the few results reported in the literature are far from conclusive.[53–55] Recent work point to energy transfer,[53] charge transfer,[54] and an optically active state at the hybrid interfaces.[55] To date, band alignments were determined from independent calculations of the TMD and perovskite layers[53,56,57] using different methods. Taking into account the accuracy of simulations based on density functional theory (DFT),[58] notably the predicted band gap, it is crucial to calculate the heterostructure as an ensemble to correctly determine the the band alignments. Here, we present such DFT calculations. We show that the $(PEA)_2PbI_4/WS_2$ stack possesses a novel band aliment, where only electron transfer between the layers is blocked. This prediction is supported by our experimental results, which point to a hole transfer from the WS_2 to the 2D perovskite, and an energy transfer in the opposite direction. Our results show that such 2D perovskite/TMD hybrid structures can be effectively used to sensitize TMDs to a particular excitation photon energy.

Results

We start with the DFT calculations, which are to the best of our knowledge, the first theoretical results which take into account the full structure and orbital hybridization of a TMDs/2D perovskite heterostructure. Fig. 2(a) shows the calculated band structure of $WS_2/(PEA)_2PbI_4$ heterostructure (the h-BN encapsulation is neglected in the calculations) where the 2D Brillouin zone of this system is indicated in panel (b) with the sampled reciprocal directions.

The band structure was projected on the majority contribution from the Mulliken analysis. This shows that the top of the valence band is mainly composed of orbitals from the PbI_4 slab, while the conduction band is dominated by the WS_2 states, as clearly seen in the density of states (DOS) plot. Consequently, a type-

II band alignment is formed between the WS_2 layer and the PbI_4 slab. Additionally, Fig. 2(c) shows a representation of the real-space highest occupied and lowest unoccupied crystal orbitals, which correspond to the valence band maximum (VBM) and conduction band minimum (CBM) respectively. The VBM at Γ is localized mostly in the PbI_4 layer, while the CBM at Ω is localized in the WS_2 layer, in accordance with the calculated DOS.

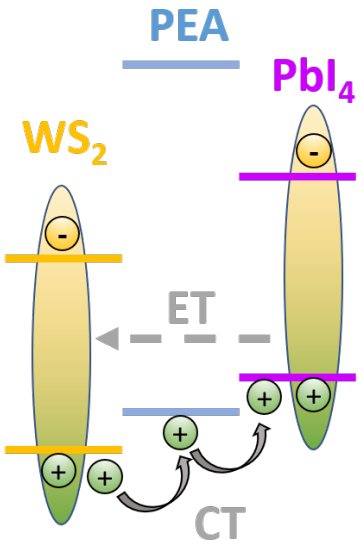

Figure 3: Summary of the band alignment in the PEPI/WS_2 heterostructure resulting from DFT calculations. The charge transfer (CT) and energy transfer (ET) paths are indicated.

In the investigated structure, the WS_2 layer is separated from the PbI_4 slab by the wide band gap PEA organic spacer. The conduction band alignment provides a barrier for electron transfer between the WS_2 and the PbI_4 layer. Indeed, based on the Hirshfeld charge analysis, we find negligible charge transfer from the WS_2 layer to the organic spacers of 0.1 e^- averaged over the whole model structure consisting of 239 atoms. Moreover, in the valence band we have an interesting situation. The peak of the PEA density of states is located around -6.5 eV, however, a closer inspection of the density of states plot (see panel (d)) reveals that there are also states related to PEA slightly above WS_2 and below PbI_4. In fact the density of these states is comparable to the WS_2 density of states close to the top of valence band. Therefore, in the valence band, the WS_2, PEA, and PbI_4 bands

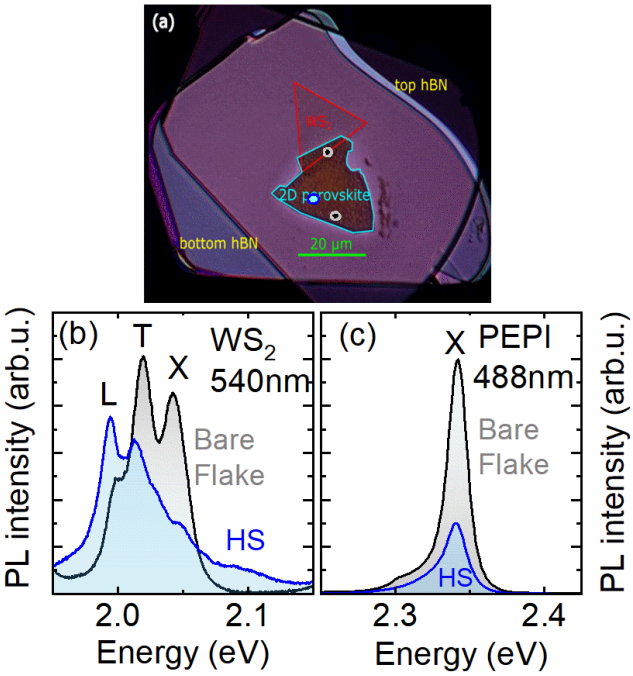

Figure 4: (a) Optical microscope image of WS_2/PEPI heterostructure sandwiched between h-BN capping layers. Color points on the image correspond to spectra shown in remaining panels. (b) PL spectra of WS_2, excited below (540 nm) the absorption band of PEPI, and (c) PL spectra of $(PEA)_2PbI_4$ (PEPI) excited above (488 nm) the absorption band of PEPI. All spectra are taken at $T = 5$ K. In panels (b-c) the spectra are taken on the heterostructure (blue) and on the bare flakes (gray).

edges form a funnel (cascade), which favorizes the transfer of photo-induced holes from WS_2 to the PbI_4 layer. Thus, stacking WS_2 with $(PEA)_2PbI_4$ leads to a novel band diagram, presented in Fig. 3, where only one type of carrier can be directly transferred between the layers, *i.e.* holes. At the same time, strong excitonic effects (in the sense of the oscillator strength) in both materials, together with their proximity, should favorize an energy transfer from the perovskite layer to the TMD layer.

To corroborate theoretical predictions, we have performed optical studies on the $WS_2/(PEA)_2PbI_4$ stack, which is placed on a Si/SiO_2 substrate, and encapsulated in h-BN to provide the highest possible optical quality and stability. Fig. 4(a) shows the optical microscope image of the sample. Three characteristic regions can be clearly distinguished, namely, the bare Ruddlesden-Popper perovskite $(PEA)_2PbI_4$, bare monolayer WS_2, and the WS_2/PEPI heterostructure area. The perovskite region is roughly $20 \times 20\,\mu m^2$ and the triangular WS_2 flake also has sides $\simeq 20\,\mu$m.

The optical properties of WS_2 monolayers are characterized by the presence of the A- and B-excitons which arise from the spin orbit splitting in the valence band. In emission, generally only the A-exciton is observed due to the large splitting ($\simeq 400$ meV) of the valence band. Fig. 4(b) shows representative PL spectra, related to the WS_2 emission, taken on the bare flake and in the heterostructure region, measured at $T = 5$ K. We can distinguish three emission features characteristic for A-exciton emission, which can be attributed to the free exciton (X), trion (T), and localized excitons (L).[59]

Even though the PL from WS_2 were collected using 540 nm excitation in Fig. 4(b) (*i.e.*, below the absorption band of PEPI), the spectra of bare WS_2 flake and the heterostructure are different. The trion to exciton ratio is changed from $\simeq$ 1.2 on the bare flake to $\simeq$ 2 on the heterostructure. In addition, the overall intensity of the WS_2 trion and exciton emission from the heterostructure is lower than on the bare flake. This finding supports the theoretical predicted hole transfer from WS_2 layer to the PbI_4 slab. The efficient hole transfer reduces the overall PL intensity in the heterostructure region. Moreover, as the WS_2 layer is intrinsically n-type,[60,61] the trion is negatively charged. The increase of T/X emission ratio in the heterostructure indicates an increased ratio of the electron/hole concentration, which is a result of the photo-induced hole transfer from WS_2 to the PEPI layer.

When the sample is excited above the absorption band of PEPI (488 nm laser), strong PL emission is observed around 2.34 eV corresponding to the dominant free exciton emission of PEPI[62–64] (Fig. 4(c)). The PEPI PL signal from the isolated flake is more intense than in the heterostructure region. However, taking into account predicted band alignment, the lower intensity in the heterostructure region cannot result from a direct charge/exciton transfer to the WS_2 layer. This suggests that the reduced PL intensity is an indication of an energy transfer process from PEPI to the WS_2 layer. However just from the PL measurement with a single excitation wave length of 488 nm it

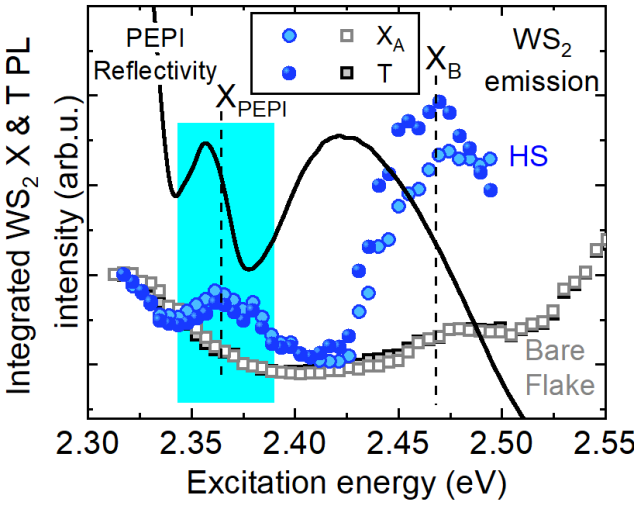

Figure 5: PL integrated intensity of X_A and T from WS_2 as a function of excitation energy in heterostructure region (blue) and on the bare flake (gray) together with reflection spectrum from PEPI (black). The excitonic resonance feature visible in reflectance spectrum corresponds to PLE feature. The reflection spectrum overlap with interference pattern resulting from h-BN encapsulation. All spectra taken at $T = 5$K

is hard to conclude if the WS_2 emission in the heterostructure area is enhanced (as expected in the case of an energy transfer from PEPI). The PL emission from WS_2 overlaps with the bound state emission from PEPI (see Fig. S1) which is visible everywhere on the PEPI flake (see Fig S2). Therefore we perform photoluminescence excitation (PLE) at 5K studies which provide further evidence of an energy transfer process from PEPI to WS_2. We varied the excitation photon energy in the range 2.3-2.6 eV while monitoring the emission intensity of the WS_2 exciton and trion recombination. The result of this experiment is shown in Fig. 5. The PLE emission from the bare WS_2 flake (gray symbols) is slightly enhanced when the excitation is resonant with the B-exciton of WS_2, due to the increased absorption.[65] The moderate increase of intensity, going to lower energies, observed below 2.4 eV, corresponds to the approaching resonant A-exciton absorption in monolayer WS_2. Crucially, for PLE in the heterostructure region, an extra feature appears at $\simeq$ 2.37 eV, *i.e.*, at an energy corresponding to the ground state exciton absorption in PEPI, also seen in the reflectivity spectrum (black line). The increased PL intensity, when exciting resonantly the exciton transition in PEPI,

is roughly the same for the trion and exciton PL from the WS_2 monolayer. This shows that the charge state of the WS_2 monolayer does not change when exciting via the PEPI. We, therefore, exclude the presence of a the charge transfer process within the heterostructure under resonant excitation conditions, and conclude that an energy transfer process is responsible for the increased excitation efficiency (increased PL intensity). This energy transfer process involves the exciton ground state in PEPI and an electron-hole continuum state in monolayer WS_2.

An additional indication of energy transfer is the strongly increased exciton and trion emission when exciting resonantly the B-exciton of WS_2 at $\simeq 2.47\,\text{eV}$. Indeed, if no energy transfer occurred, the exciton and trion PL intensity in the heterostructure region would be the same as for the isolated monolayer. Increased PL intensity indicates another energy transfer process involving the B-exciton in monolayer WS_2 and probably excited exciton states (2s, 3s, ...) in PEPI.[66–68] The large enhancement in the WS_2 exciton and trion PL intensity in Fig. 5 shows that this energy transfer process is more efficient than the energy transfer when exciting the PEPI exciton ground state at 2.37 eV. Since the energy transfer efficiency of a Förster or Dexter type is proportional to the product of the oscillator strengths of the energy donor and acceptor, our results suggest that this product is significantly larger for PEPI excited excitons states and the WS_2 B-exciton than for WS_2 free carriers and PEPI 1s state. Overall, the results presented in Fig. 5 show an efficient sensitization of the WS_2 monolayer via energy transfer from PEPI.

Finally, we consider the nature of the energy transfer process. In the heterostructure, the centers of the WS_2 and PbI_4 layers are separated by about 1-1.5 nm. This distance is often considered as limiting for Dexter type processes, but not for Förster.[32–39] Moreover, the Dexter type mechanism involves an exchange of carriers between states. Hence, in addition to an overlap of the emission and absorption energies, the Dexter mechanism requires an overlap of the wave-functions of the donor and acceptor states. As the DFT calculations show that the wave-function overlap is negligible, we conclude that the Förster process is the most probable mechanism for the energy transfer.

Conclusions

We have presented the evidence for both charge and energy transfer in the $(PEA)_2PbI_4/WS_2$ heterostructure at low temperature. Due to particular band alignment between the PEPI and WS_2 layers, only the hole transfer is present from the TMD to the 2D perovskite. Simultaneously, the electron exchange between the layer is completely blocked. However, the excitation can be transferred from $(PEA)_2PbI_4$ to WS_2 via an energy transfer process, which is especially efficient close to the B-exciton resonance in WS_2. This is confirmed by PLE studies showing that WS_2 monolayer can be effectively sensitized by the $(PEA)_2PbI_4$ 2D perovskite.

Methods

Synthesis and sample preparation

The device has a multilayer structure composed of a boron nitride (h-BN) top layer ($\sim 100\,\text{nm}$), a WS_2 monolayer, a $(PEA)_2PbI_4$ perovskite ($\simeq 50\,\text{nm}$), and an h-BN bottom layer ($\simeq 120\,\text{nm}$). The WS_2 monolayer is grown by the chemical vapor deposition.[69] Both $(PEA)_2PbI_4$ perovskite and boron nitride flakes are exfoliated from their bulk crystals. Single crystals of $(PEA)_2PbI_4$ were grown at room temperature using the same layered solution crystal growth technique as used in our previous work.[70] To avoid the degradation of $(PEA)_2PbI_4$ perovskite in the ambient condition, the cleavage, transfer, and stacking are all carried out in an argon-filled glove box with a trace amount of H_2O and O_2 (both less than 0.1 ppm). During the transfer process, the top h-BN layer is picked up by a polycarbonate film (PC) at 80°C, then WS_2 monolayer and $(PEA)_2PbI_4$ perovskite flakes are picked up by the top h-BN layer at 110 and 40°C, respectively. Care was

taken to minimize the heating process to avoid the thermal degradation of the perovskite. The PC on the sandwiched structure is then quickly dissolved in chloroform within 3 minutes. We have confirmed that the optical properties of the perovskite are not affected by the solution process after being sandwiched between WS_2 and h-BN.

DFT calculations

A bi-layer model structure of WS_2@$(PEA)_2PbI_4$ was created in the Virtual NanoLab[71] with minimal strain on the individual layers, resulting in a superstructure with 239 atoms. This model structure was fully relaxed using FHI-aims[72] employing the PBE functional[73] on tight tier 1 numeric atom-centered orbitals, including the non-local many-body dispersion correction (MBD-nl)[74,75] and scalar relativistic corrections (ZORA) on a $6 \times 6 \times 1$ Γ-centered k-grid. The electronic band structure, the Mulliken-projections, and the density of states were calculated including spin-orbit coupling (SOC) and considering the dipole correction.

Optical measurements

The sample was mounted on the cold finger of a liquid helium cooled cryostat. Both, reflectivity and PL measurements were performed on the home-built setup at the temperature of around 5 K. The excitation source was halogen lamp (for reflectivity), and continuous wave 488 nm gas laser or second harmonic of a Ti:sapphire laser (for PL). The white light/laser beam was focused on the sample by a 50× microscope objective with a numerical aperture of 0.55, resulting in the spot size of $\simeq 1\mu$m. The signal from the sample was collected by the same objective, directed to the 0.5 m long monochromator and detected by liquid nitrogen cooled CCD camera. For PL, the laser beam was filtered out by the long pass 488 nm or 550 nm edge filter. Spatial PL maps with the step of 1μm along the x and y axes, were possible with the use of an automated xy translation stages on which the cryostat was mounted. PLE experiments were performed using the same setup as the PL measurements at 5 K. The excitation source was the second harmonic of a Ti:sapphire laser with a repetition rate of 80 MHz and temporal pulse width of 300 fs. The laser signal was filtered out by the 550 nm long pass edge filter before entering the monochromator and CCD camera.

Acknowledgments

M.E.K. was supported by The Netherlands Organization for Scientific Research (NWO Graduate Programme 2013, No. 022.005.006) PP appreciates support from National Science Centre Poland within the OPUS program (grant no. 2019/33/B/ST3/01915). This work was partially supported by OPEP project, which received funding from the ANR-10-LABX-0037-NEXT.This is a publication of the FOM-focus Group "Next Generation Organic Photovoltaics," financed by the Netherlands Organization for Scientific Research (NWO) and participating in the Dutch Institute for Fundamental Energy Research (DIFFER). S. A. acknowledges the financial support of the Netherlands Organization for Scientific Research (NWO graduate project 2013, No 022.005.006). The Polish participation in European Magnetic Field Laboratory is supported by the DIR/WK/2018/07 grant from Ministry of Science and Higher Education, Poland. AK, RK and KF gratefully acknowledge the Gauss Centre for Supercomputing e.V. (www.gauss-centre.eu) for funding this project by providing computing time through the John von Neumann Institute for Computing (NIC) on the GCS Supercomputer JUWELS at Jülich Supercomputing Centre (JSC). Furthermore, AK, RK and KF gratefully acknowledge the GWK support for funding this project by providing computing time through the Center for Information Services and HPC (ZIH) at TU Dresden. AK acknowledges the financial support from Deutsche Forschungsgemeinschaft (DFG, German Research Foundation) within SFB1415 project number 417590517 and the association with the SPP2244 (2DMP)

References

(1) Tan, C.; Cao, X.; Wu, X.-J.; He, Q.; Yang, J.; Zhang, X.; Chen, J.; Zhao, W.; Han, S.; Nam, G.-H., et al. Recent advances in ultrathin two-dimensional nanomaterials. *Chemical reviews* **2017**, *117*, 6225–6331.

(2) Geng, D.; Yang, H. Y. Recent advances in growth of novel 2D materials: beyond graphene and transition metal dichalcogenides. *Advanced Materials* **2018**, *30*, 1800865.

(3) Novoselov, K. S.; Geim, A. K.; Morozov, S. V.; Jiang, D.; Zhang, Y.; Dubonos, S. V.; Grigorieva, I. V.; Firsov, A. A. Electric field effect in atomically thin carbon films. *science* **2004**, *306*, 666–669.

(4) Geim, A. K. Nobel Lecture: Random walk to graphene. *Reviews of Modern Physics* **2011**, *83*, 851.

(5) Mak, K. F.; Lee, C.; Hone, J.; Shan, J.; Heinz, T. F. Atomically thin MoS 2: a new direct-gap semiconductor. *Physical review letters* **2010**, *105*, 136805.

(6) Xu, X.; Yao, W.; Xiao, D.; Heinz, T. F. Spin and pseudospins in layered transition metal dichalcogenides. *Nature Physics* **2014**, *10*, 343–350.

(7) Chen, Y.; Sun, Y.; Peng, J.; Tang, J.; Zheng, K.; Liang, Z. 2D Ruddlesden–Popper perovskites for optoelectronics. *Advanced Materials* **2018**, *30*, 1703487.

(8) Straus, D. B.; Kagan, C. R. Electrons, excitons, and phonons in two-dimensional hybrid perovskites: connecting structural, optical, and electronic properties. *The journal of physical chemistry letters* **2018**, *9*, 1434–1447.

(9) Castellanos-Gomez, A.; Vicarelli, L.; Prada, E.; Island, J. O.; Narasimha-Acharya, K.; Blanter, S. I.; Groenendijk, D. J.; Buscema, M.; Steele, G. A.; Alvarez, J., et al. Isolation and characterization of few-layer black phosphorus. *2D Materials* **2014**, *1*, 025001.

(10) Gibertini, M.; Koperski, M.; Morpurgo, A.; Novoselov, K. Magnetic 2D materials and heterostructures. *Nature nanotechnology* **2019**, *14*, 408–419.

(11) Liu, Y.; Weiss, N. O.; Duan, X.; Cheng, H.-C.; Huang, Y.; Duan, X. Van der Waals heterostructures and devices. *Nature Reviews Materials* **2016**, *1*, 1–17.

(12) Tang, Y.; Li, L.; Li, T.; Xu, Y.; Liu, S.; Barmak, K.; Watanabe, K.; Taniguchi, T.; MacDonald, A. H.; Shan, J., et al. Simulation of Hubbard model physics in WSe 2/WS 2 moiré superlattices. *Nature* **2020**, *579*, 353–358.

(13) Raja, A.; Chaves, A.; Yu, J.; Arefe, G.; Hill, H. M.; Rigosi, A. F.; Berkelbach, T. C.; Nagler, P.; Schüller, C.; Korn, T., et al. Coulomb engineering of the bandgap and excitons in two-dimensional materials. *Nature communications* **2017**, *8*, 1–7.

(14) Geim, A. K.; Grigorieva, I. V. Van der Waals heterostructures. *Nature* **2013**, *499*, 419–425.

(15) Yu, H.; Liu, G.-B.; Tang, J.; Xu, X.; Yao, W. Moiré excitons: From programmable quantum emitter arrays to spin-orbit–coupled artificial lattices. *Science advances* **2017**, *3*, e1701696.

(16) Zhang, N.; Surrente, A.; Baranowski, M.; Maude, D. K.; Gant, P.; Castellanos-Gomez, A.; Plochocka, P. Moiré intralayer excitons in a MoSe2/MoS2 heterostructure. *Nano letters* **2018**, *18*, 7651–7657.

(17) Scuri, G. et al. Electrically Tunable Valley Dynamics in Twisted WSe2/WSe2 Bilayers. *Physical Review Letters* **2020**, *124*.

(18) Sung, J. et al. Broken mirror symmetry in excitonic response of reconstructed domains in twisted MoSe2/MoSe2 bilayers.

Nature Nanotechnology **2020**, *15*, 750–754.

(19) Rivera, P.; Schaibley, J. R.; Jones, A. M.; Ross, J. S.; Wu, S.; Aivazian, G.; Klement, P.; Seyler, K.; Clark, G.; Ghimire, N. J., et al. Observation of long-lived interlayer excitons in monolayer MoSe 2–WSe 2 heterostructures. *Nature communications* **2015**, *6*, 1–6.

(20) Miller, B.; Steinhoff, A.; Pano, B.; Klein, J.; Jahnke, F.; Holleitner, A.; Wurstbauer, U. Long-lived direct and indirect interlayer excitons in van der Waals heterostructures. *Nano letters* **2017**, *17*, 5229–5237.

(21) Baranowski, M.; Surrente, A.; Klopotowski, L.; Urban, J.; Zhang, N.; Maude, D. K.; Wiwatowski, K.; Mackowski, S.; Kung, Y.-C.; Dumcenco, D., et al. Probing the interlayer exciton physics in a MoS2/MoSe2/MoS2 van der Waals heterostructure. *Nano letters* **2017**, *17*, 6360–6365.

(22) Surrente, A.; Kłopotowski, Ł.; Zhang, N.; Baranowski, M.; Mitioglu, A. A.; Ballottin, M. V.; Christianen, P. C.; Dumcenco, D.; Kung, Y.-C.; Maude, D. K., et al. Intervalley scattering of interlayer excitons in a mos2/mose2/mos2 heterostructure in high magnetic field. *Nano letters* **2018**, *18*, 3994–4000.

(23) Ciarrocchi, A.; Unuchek, D.; Avsar, A.; Watanabe, K.; Taniguchi, T.; Kis, A. Polarization switching and electrical control of interlayer excitons in two-dimensional van der Waals heterostructures. *Nature photonics* **2019**, *13*, 131–136.

(24) Nagler, P.; Ballottin, M. V.; Mitioglu, A. A.; Mooshammer, F.; Paradiso, N.; Strunk, C.; Huber, R.; Chernikov, A.; Christianen, P. C.; Schüller, C., et al. Giant magnetic splitting inducing near-unity valley polarization in van der Waals heterostructures. *Nature communications* **2017**, *8*, 1–6.

(25) Seyler, K. L.; Rivera, P.; Yu, H.; Wilson, N. P.; Ray, E. L.; Mandrus, D. G.; Yan, J.; Yao, W.; Xu, X. Signatures of moiré-trapped valley excitons in MoSe 2/WSe 2 heterobilayers. *Nature* **2019**, *567*, 66–70.

(26) Tran, K. et al. Evidence for moiré excitons in van der Waals heterostructures. *Nature* **2019**, *567*, 71–75.

(27) Wang, Z.; Rhodes, D. A.; Watanabe, K.; Taniguchi, T.; Hone, J. C.; Shan, J.; Mak, K. F. Evidence of high-temperature exciton condensation in two-dimensional atomic double layers. *Nature* **2019**, *574*, 76–80.

(28) Regan, E. C.; Wang, D.; Jin, C.; Utama, M. I. B.; Gao, B.; Wei, X.; Zhao, S.; Zhao, W.; Zhang, Z.; Yumigeta, K., et al. Mott and generalized Wigner crystal states in WSe 2/WS 2 moiré superlattices. *Nature* **2020**, *579*, 359–363.

(29) Gong, C.; Zhang, H.; Wang, W.; Colombo, L.; Wallace, R. M.; Cho, K. Band alignment of two-dimensional transition metal dichalcogenides: Application in tunnel field effect transistors. *Applied Physics Letters* **2013**, *103*, 053513.

(30) Alexeev, E. M.; Ruiz-Tijerina, D. A.; Danovich, M.; Hamer, M. J.; Terry, D. J.; Nayak, P. K.; Ahn, S.; Pak, S.; Lee, J.; Sohn, J. I., et al. Resonantly hybridized excitons in moiré superlattices in van der Waals heterostructures. *Nature* **2019**, *567*, 81–86.

(31) Jin, C.; Regan, E. C.; Yan, A.; Utama, M. I. B.; Wang, D.; Zhao, S.; Qin, Y.; Yang, S.; Zheng, Z.; Shi, S., et al. Observation of moiré excitons in WSe 2/WS 2 heterostructure superlattices. *Nature* **2019**, *567*, 76–80.

(32) Fŏrster, T. 10th Spiers Memorial Lecture. Transfer mechanisms of electronic excitation. *Discuss. Faraday Soc.* **1959**, *27*, 7–17.

(33) Dexter, D. L. A Theory of Sensitized Luminescence in Solids. *The Journal of Chemical Physics* **1953**, *21*, 836–850.

(34) Baldo, M. A.; Thompson, M. E.; Forrest, S. R. High-efficiency fluorescent organic light-emitting devices using a phosphorescent sensitizer. *Nature* **2000**, *403*, 750–753.

(35) Becker, K.; Lupton, J. M.; Müller, J.; Rogach, A. L.; Talapin, D. V.; Weller, H.; Feldmann, J. Electrical control of Förster energy transfer. *Nature Materials* **2006**, *5*, 777–781.

(36) Achermann, M.; Petruska, M. A.; Kos, S.; Smith, D. L.; Koleske, D. D.; Klimov, V. I. Energy-transfer pumping of semiconductor nanocrystals using an epitaxial quantum well. *Nature* **2004**, *429*, 642–646.

(37) Lyo, S. K. Energy transfer of excitons between quantum wells separated by a wide barrier. *Physical Review B* **2000**, *62*, 13641–13656.

(38) Kozawa, D.; Carvalho, A.; Verzhbitskiy, I.; Giustiniano, F.; Miyauchi, Y.; Mouri, S.; Neto, A. H. C.; Matsuda, K.; Eda, G. Evidence for Fast Interlayer Energy Transfer in MoSe2/WS2 Heterostructures. *Nano Letters* **2016**, *16*, 4087–4093.

(39) Hu, Z.; Hernández-Martínez, P. L.; Liu, X.; Amara, M.-R.; Zhao, W.; Watanabe, K.; Taniguchi, T.; Demir, H. V.; Xiong, Q. Trion-Mediated Förster Resonance Energy Transfer and Optical Gating Effect in WS2/hBN/MoSe2 Heterojunction. *ACS Nano* **2020**, *14*, 13470–13477.

(40) Liu, X.; Pei, J.; Hu, Z.; Zhao, W.; Liu, S.; Amara, M.-R.; Watanabe, K.; Taniguchi, T.; Zhang, H.; Xiong, Q. Manipulating Charge and Energy Transfer between 2D Atomic Layers via Heterostructure Engineering. *Nano Letters* **2020**, *20*, 5359–5366.

(41) Zhang, L.; Sharma, A.; Zhu, Y.; Zhang, Y.; Wang, B.; Dong, M.; Nguyen, H. T.; Wang, Z.; Wen, B.; Cao, Y., et al. Efficient and Layer-Dependent Exciton Pumping across Atomically Thin Organic–Inorganic Type-I Heterostructures. *Advanced Materials* **2018**, *30*, 1803986.

(42) Xu, W.; Kozawa, D.; Liu, Y.; Sheng, Y.; Wei, K.; Koman, V. B.; Wang, S.; Wang, X.; Jiang, T.; Strano, M. S., et al. Determining the optimized interlayer separation distance in vertical stacked 2D WS2: hBN: MoS2 heterostructures for exciton energy transfer. *Small* **2018**, *14*, 1703727.

(43) Even, J.; Pedesseau, L.; Katan, C. Understanding Quantum Confinement of Charge Carriers in Layered 2D Hybrid Perovskites. *ChemPhysChem* **2014**, *15*, 3733–3741.

(44) Katan, C.; Mercier, N.; Even, J. Quantum and Dielectric Confinement Effects in Lower-Dimensional Hybrid Perovskite Semiconductors. *Chemical Reviews* **2019**, *119*, 3140–3192.

(45) Blancon, J.-C. et al. Extremely efficient internal exciton dissociation through edge states in layered 2D perovskites. *Science* **2017**, *355*, 1288–1292.

(46) Blancon, J.-C. et al. Scaling law for excitons in 2D perovskite quantum wells. *Nature Communications* **2018**, *9*.

(47) Yu, Z.; Ong, Z.-Y.; Li, S.; Xu, J.-B.; Zhang, G.; Zhang, Y.-W.; Shi, Y.; Wang, X. Analyzing the carrier mobility in transition-metal dichalcogenide MoS2 field-effect transistors. *Advanced Functional Materials* **2017**, *27*, 1604093.

(48) Fallahazad, B.; Movva, H. C.; Kim, K.; Larentis, S.; Taniguchi, T.; Watanabe, K.; Banerjee, S. K.; Tutuc, E. Shubnikov–de Haas Oscillations of High-Mobility Holes in Monolayer and BilayerWSe2: Landau Level Degeneracy, Effective Mass, and Negative Compressibility. *Physical Review Letters* **2016**, *116*.

(49) Song, X.; Liu, X.; Yu, D.; Huo, C.; Ji, J.; Li, X.; Zhang, S.; Zou, Y.; Zhu, G.; Wang, Y., et al. Boosting two-dimensional MoS2/CsPbBr3 photodetectors via enhanced light absorbance and interfacial carrier separation. *ACS applied materials & interfaces* **2018**, *10*, 2801–2809.

(50) Fang, Q.; Shang, Q.; Zhao, L.; Wang, R.; Zhang, Z.; Yang, P.; Sui, X.; Qiu, X.; Liu, X.; Zhang, Q., et al. Ultrafast charge transfer in perovskite nanowire/2D transition metal dichalcogenide heterostructures. *The journal of physical chemistry letters* **2018**, *9*, 1655–1662.

(51) Kang, D.-H.; Pae, S. R.; Shim, J.; Yoo, G.; Jeon, J.; Leem, J. W.; Yu, J. S.; Lee, S.; Shin, B.; Park, J.-H. An Ultrahigh-Performance Photodetector based on a Perovskite–Transition-Metal-Dichalcogenide Hybrid Structure. *Advanced Materials* **2016**, *28*, 7799–7806.

(52) Wu, H.; Si, H.; Zhang, Z.; Kang, Z.; Wu, P.; Zhou, L.; Zhang, S.; Zhang, Z.; Liao, Q.; Zhang, Y. All-Inorganic Perovskite Quantum Dot-Monolayer MoS2 Mixed-Dimensional van der Waals Heterostructure for Ultrasensitive Photodetector. *Advanced Science* **2018**, *5*, 1801219.

(53) Zhang, Q.; Linardy, E.; Wang, X.; Eda, G. Excitonic Energy Transfer in Heterostructures of Quasi-2D Perovskite and Monolayer WS2. *ACS Nano* **2020**,

(54) Chen, Y.; Liu, Z.; Li, J.; Cheng, X.; Ma, J.; Wang, H.; Li, D. Robust Interlayer Coupling in Two-Dimensional Perovskite/Monolayer Transition Metal Dichalcogenide Heterostructures. *ACS Nano* **2020**,

(55) Yang, A.; Blancon, J.-C.; Jiang, W.; Zhang, H.; Wong, J.; Yan, E.; Lin, Y.-R.; Crochet, J.; Kanatzidis, M. G.; Jariwala, D.; Low, T.; Mohite, A. D.; Atwater, H. A. Giant Enhancement of Photoluminescence Emission in WS2-Two-Dimensional Perovskite Heterostructures. *Nano Letters* **2019**, *19*, 4852–4860.

(56) Traore, B.; Pedesseau, L.; Assam, L.; Che, X.; Blancon, J.-C.; Tsai, H.; Nie, W.; Stoumpos, C. C.; Kanatzidis, M. G.; Tretiak, S., et al. Composite nature of layered hybrid perovskites: assessment on quantum and dielectric confinements and band alignment. *ACS nano* **2018**, *12*, 3321–3332.

(57) Kang, J.; Tongay, S.; Zhou, J.; Li, J.; Wu, J. Band offsets and heterostructures of two-dimensional semiconductors. *Applied Physics Letters* **2013**, *102*, 012111.

(58) Crowley, J. M.; Tahir-Kheli, J.; Goddard III, W. A. Resolution of the band gap prediction problem for materials design. *The journal of physical chemistry letters* **2016**, *7*, 1198–1203.

(59) Jadczak, J.; Kutrowska-Girzycka, J.; Kapuściński, P.; Huang, Y.; Wójs, A.; Bryja, z. Probing of free and localized excitons and trions in atomically thin WSe2, WS2, MoSe2 and MoS2 in photoluminescence and reflectivity experiments. *Nanotechnology* **2017**, *28*, 395702.

(60) Feng, S.; Cong, C.; Konabe, S.; Zhang, J.; Shang, J.; Chen, Y.; Zou, C.; Cao, B.; Wu, L.; Peimyoo, N., et al. Engineering valley polarization of monolayer WS2: a physical doping approach. *Small* **2019**, *15*, 1805503.

(61) Zhu, B.; Chen, X.; Cui, X. Exciton binding energy of monolayer WS 2. *Scientific reports* **2015**, *5*, 9218.

(62) Hong, X.; Ishihara, T.; Nurmikko, A. Dielectric confinement effect on excitons in PbI 4-based layered semiconductors. *Physical Review B* **1992**, *45*, 6961.

(63) Straus, D. B.; Iotov, N.; Gau, M. R.; Zhao, Q.; Carroll, P. J.; Kagan, C. R. Longer cations increase energetic disorder in excitonic 2D hybrid perovskites. *The*

journal of physical chemistry letters **2019**, *10*, 1198–1205.

(64) Straus, D. B.; Hurtado Parra, S.; Iotov, N.; Zhao, Q.; Gau, M. R.; Carroll, P. J.; Kikkawa, J. M.; Kagan, C. R. Tailoring Hot Exciton Dynamics in 2D Hybrid Perovskites through Cation Modification. *ACS nano* **2020**, *14*, 3621–3629.

(65) Kozawa, D.; Kumar, R.; Carvalho, A.; Amara, K. K.; Zhao, W.; Wang, S.; Toh, M.; Ribeiro, R. M.; Neto, A. C.; Matsuda, K., et al. Photocarrier relaxation pathway in two-dimensional semiconducting transition metal dichalcogenides. *Nature communications* **2014**, *5*, 1–7.

(66) Feldstein, D.; Perea-Causin, R.; Wang, S.; Dyksik, M.; Watanabe, K.; Taniguchi, T.; Plochocka, P.; Malic, E. Microscopic Picture of Electron–Phonon Interaction in Two-Dimensional Halide Perovskites. *The Journal of Physical Chemistry Letters* **2020**, *11*, 9975–9982.

(67) Urban, J. M.; Chehade, G.; Dyksik, M.; Menahem, M.; Surrente, A.; Trippé-Allard, G.; Maude, D. K.; Garrot, D.; Yaffe, O.; Deleporte, E., et al. Revealing Excitonic Phonon Coupling in (PEA) 2 (MA) n- 1Pb n I3 n+ 1 2D Layered Perovskites. *The Journal of Physical Chemistry Letters* **2020**, *11*, 5830–5835.

(68) Dyksik, M.; Duim, H.; Zhu, X.; Yang, Z.; Gen, M.; Kohama, Y.; Adjokatse, S.; Maude, D. K.; Loi, M. A.; Egger, D. A., et al. Broad Tunability of Carrier Effective Masses in Two-Dimensional Halide Perovskites. *ACS Energy Letters* **2020**, *5*, 3609–3616.

(69) Zhou, J. et al. A library of atomically thin metal chalcogenides. *Nature* **2018**, *556*, 355–359.

(70) Kamminga, M. E.; Fang, H.-H.; Filip, M. R.; Giustino, F.; Baas, J.; Blake, G. R.; Loi, M. A.; Palstra, T. T. M. Confinement Effects in Low-Dimensional Lead Iodide Perovskite Hybrids. *Chemistry of Materials* **2016**, *28*, 4554–4562.

(71) Stradi, D.; Jelver, L.; Smidstrup, S.; Stokbro, K. Method for determining optimal supercell representation of interfaces. *Journal of Physics: Condensed Matter* **2017**, *29*, 185901.

(72) Blum, V.; Gehrke, R.; Hanke, F.; Havu, P.; Havu, V.; Ren, X.; Reuter, K.; Scheffler, M. Ab initio molecular simulations with numeric atom-centered orbitals. *Computer Physics Communications* **2009**, *180*, 2175–2196.

(73) Perdew, J. P.; Burke, K.; Ernzerhof, M. Generalized Gradient Approximation Made Simple. *Physical Review Letters* **1996**, *77*, 3865–3868.

(74) Tkatchenko, A.; Ambrosetti, A.; DiStasio, R. A. Interatomic methods for the dispersion energy derived from the adiabatic connection fluctuation-dissipation theorem. *The Journal of Chemical Physics* **2013**, *138*, 074106.

(75) Hermann, J.; Tkatchenko, A. Density Functional Model for van der Waals Interactions: Unifying Many-Body Atomic Approaches with Nonlocal Functionals. *Physical Review Letters* **2020**, *124*.